Journal of Sound and Vibration (1997) **200**(4), 519–530

FINITE ELEMENT ANALYSIS OF THE PROPAGATION OF ACOUSTIC WAVES ALONG WAVEGUIDES IMMERSED IN WATER

A.-C. Hladky-Hennion and P. Langlet

IEMN, *Département ISEN*, 41 *Boulevard Vauban*, 59046 *Lille cedex*, *France*

and

M. de Billy

Groupe de Physique des Solides, *Université Paris* 7, *Tour* 23, 2 *Place Jussieu*, 75251 *Paris cedex* 05, *France*

(*Received* 3 *April* 1996, *and in final form* 11 *September* 1996)

The finite element approach has previously been used, with the help of the ATILA code, to model the propagation of acoustic waves in waveguides [A.-C. Hladky-Hennion, *Journal of Sound and Vibration* **194**, 119–136 (1996)]. In this paper an extension of the technique to the analysis of the propagation of acoustic waves in immersed waveguides is presented. In the proposed approach, the problem is reduced to a bidimensional problem, in which only the cross-section of the guide and the surrounding fluid domain are meshed by using finite elements. Then, wedges, the top angles of which vary, are studied and the finite element results of the wedge wave speed are compared with experimental results. Finally, the conclusion indicates a way to extend this approach to waveguides of any cross-section.

1. INTRODUCTION

Flexural wedge waves, propagating along the tip of an ideal sharp elastic wedge, attracted considerable interest in the 1970s, because these waves are dispersionless, their propagation speed is lower than the Rayleigh wave speed and the acoustic energy is confined at the tip of the wedge guide. As the boundary conditions of the problem are complex, it is difficult to use a simple model to study the propagation of acoustic waves in guides. Ash *et al*. [1] suggested the use of a simple edge as a guiding structure. Then, Moss *et al*. [2] established an analytical model limited to the simple geometry of linear wedges. Lagasse [3] applied the finite element method to analyze the propagation of acoustic waves in an infinite waveguide of arbirary cross-section in air. The technique is original because the problem is reduced to a bidimensional problem, in which only the cross-section of the guide is meshed by using finite elements. Lately, this technique has also been used in the case of curved waveguides [4]. Recently, wedge waves have again attracted interest: Krylov *et al*. have developed an approximate analytical solution [5] for wedges embedded in water, the top angle of which is small, whereas Chamuel [6, 7] has measured the effect of water loading on wedge waves along the apex of an immersed acute-angle solid wedge for applications in geophysics and underwater acoustics.

To the authors' knowledge, theoretical or numerical modelling of the immersed solid wedge has not yet been developed in the general case. Thus, the use of the finite element method to tackle the problem can strongly broaden the designer's possibilities, particularly

0022–460X/97/090519 + 12 $25.00/0/sv960749

because it allows the modelling of any cross-sectional geometry, by simply building specific meshes, without any new algebraic development.

In this paper the extension of the finite element technique previously described [4] to the case of immersed waveguides is presented. First, the theoretical formulation is presented for immersed linear waveguides, which has been incorporated in the ATILA finite element code [8]. The problem is reduced to a bidimensional problem, in which only the cross-section of the guide and the surrounding fluid domain are meshed by using finite elements. Then, the wave speed of a wedge, the top angle of which is variable, is studied, and the finite element results are compared to experimental results, demonstrating the accuracy of the model. In this paper, the problem is limited to the propagating waves along the wedge without re-emission in the fluid. Physical effects are observed and are accurately analyzed. Finally, the conclusion indicates a way to extend this approach to waveguides of any cross-section, for applications in signal processing devices, in geophysics and in underwater acoustics, as well as in solid surface physics.

2. THEORETICAL FORMULATION FOR A LINEAR IMMERSED WAVEGUIDE

2.1. DESCRIPTION OF THE PROBLEM

An acoustic wave, characterized by its wavenumber k_z, is propagating along a uniform, infinite and immersed waveguide, in the z direction. The displacement field vector $\mathbf{u}$ in the solid domain is written as

$$\mathbf{u} = \begin{pmatrix} u_x(x, y) \\ u_y(x, y) \\ \mathrm{j}u_z(x, y) \end{pmatrix} \mathrm{e}^{\mathrm{j}k_z z}. \tag{1}$$

To assure the quadrature between two in-plane displacements, the displacement component in the waveguide direction is multiplied by the imaginary unit j [3]. The time dependence ($\mathrm{e}^{-\mathrm{j}\omega t}$) is implicit in the equations. In the same way, the pressure in the fluid domain is written as

$$p = p(x, y)\, \mathrm{e}^{\mathrm{j}k_z z}. \tag{2}$$

2.2. FINITE ELEMENT SYSTEM OF EQUATIONS

Because the section of the waveguide is uniform in the z direction, it is possible to solve the problem with the help of a bidimensional mesh and to reconstitute the whole solution [4, 9].

A unit length of the waveguide is meshed with the help of the finite element method. The whole domain contains a solid domain Ω_s and a fluid domain Ω_f separated by the S_i interface surface. The fluid domain is limited by the S_r radiating surface. The whole domain is split into elements connected by nodes. The trace of the tridimensional solid domain Ω_s in the x–y plane is the surface S_s and the trace of the tridimensional fluid domain Ω_f in the x–y plane is the surface S_f. So, in the x–y plane (see Figure 1 for notations), the whole domain is split into the following parts: the fluid domain S_f and the solid domain S_s; the interface line l_i, which is the trace of the S_i surface in the x–y plane, separating the fluid and the solid domains; the radiating elements on the l_r line, which is the trace of the S_r surface in the x–y plane, limiting the finite element mesh. On this line, a non-reflecting condition is applied, the pressure field being assumed to be essentially monopolar [10].

The general system of equations associated to this problem is [8]

$$\begin{bmatrix} [K]-\omega^2[M] & -[L] \\ -\rho_f^2 c_f^2 \omega^2 [L]^T & [H]-\omega^2[M_1] \end{bmatrix} \begin{pmatrix} \mathbf{U} \\ \mathbf{P} \end{pmatrix} = \begin{pmatrix} \mathbf{F} \\ \rho_f c_f^2 \boldsymbol{\phi} \end{pmatrix}, \tag{3}$$

where $[K]$ is the stiffness matrix, whereas $[M]$ is the mass matrix in the solid domain Ω_s. $[H]$ is the compressibility matrix and $[M_1]$ is the mass matrix in the fluid domain $\boldsymbol{\Omega}_f$. $[L]$ is the interface matrix, which represents the coupling between the fluid and the solid on the S_i surface. ρ_f and c_f are, respectively, the density and the sound speed in the fluid. $\mathbf{F}$ contains the nodal values of the applied forces, which are equal to zero. $\boldsymbol{\phi}$ contains the nodal values of the pressure normal derivative on the external fluid boundary. By a modal analysis, the resolution of the system gives ω, the angular frequency and the corresponding eigenvectors: $\mathbf{U}$, the vector of the nodal values of the displacement field and $\mathbf{P}$, the vector of the nodal values of the pressure field.

The non-reflecting condition on the external fluid boundary allows one to limit the finite element mesh. As the pressure is assumed to be monopolar, the relation between the vector of the nodal values of the normal pressure derivative $\boldsymbol{\phi}$ and the vector of the nodal values of the pressure field $\mathbf{P}_\infty$ on the external fluid boundary is [10, 11]

$$\boldsymbol{\phi} = -[\tfrac{1}{2} - \mathrm{j}k_r R][D]\mathbf{P}_\infty / R, \tag{4}$$

where R is the radius of the external fluid boundary, k_r is the radial component of the wavevector and $[D]$ is the monopolar radiating matrix, which depends only on the interpolation functions in the elements. This non-reflecting condition is valid if the external fluid boundary is outside the near field area ($k_f R \gg 1$). In that case, the decreasing of the pressure field is proportional to $\mathrm{e}^{\mathrm{j}k_r R}/\sqrt{R}$.

2.3. MODIFICATION OF THE SYSTEM

2.3.1 *Solid domain*

This part is detailed in reference [4]. Thus, only the main results are reproduced here. Classically, in the finite element method for a solid structure, the three components of the displacement field vector $\mathbf{u}$ in the x, y and z directions (equation (1), are written with the help of the interpolation functions $[N]$ and of the vector of the nodal values of the displacement field $\mathbf{U}$ [4, 8, 9]. Thus, the stiffness matrix and the mass matrix of equation (3) are modified. The stiffness matrix $[K]$ is k_z dependent and can be written as [4]

$$[K] = [K_0] + k_z[K_1] + k_z^2[K_2], \tag{5}$$

where $[K_0]$, $[K_1]$ and $[K_2]$ are all three real symmetric matrices because the material is lossless. The $[K_0]$, $[K_1]$ and $[K_2]$ matrices are independent of k_z. The stiffness matrix is calculated by integrating over the x and y variables on the cross-section S_s. Thus, the displacement field is z dependent but a bidimensional mesh, depending on x and y, is

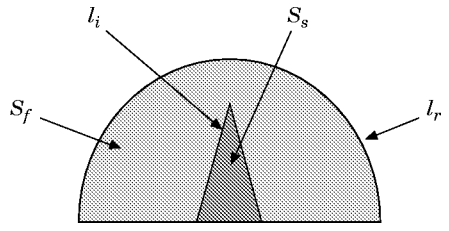

Figure 1. Traces of the finite element domains in the x–y plane.

sufficient to calculate the stiffness matrix. In all of the following examples, isoparametric elements are used, with a quadratic interpolation along the element sides.

In the same way, the mass matrix $[M]$ is calculated by considering the displacement field of equation (1). The mass matrix is modified but is k_z independent [4].

2.3.2. *Fluid domain*

By following the same formalism as in the case of the solid domain, the pressure field p is written as

$$p = [N_p]\mathbf{P} = [N_p[x, y)]\, \mathrm{e}^{\mathrm{j}k_z z}\mathbf{P}, \tag{6}$$

where $[N_p(x, y)]$ is the interpolation function in the fluid domain. The gradient of the pressure field, which is needed for the compressibility matrix, is

$$\overrightarrow{\mathbf{grad}}\, p = [B_p]\mathbf{P}. \tag{7}$$

The $[B_p]$ matrix results in the assembling of the $[B_{pi}]$ matrices, which are the matrices of the spatial derivative of the interpolation functions for the node i are written as

$$[B_{pi}] = \begin{bmatrix} [\partial[N_{pi}(x, y)]/\partial x \\ [\partial[N_{pi}(x, y)]/\partial y \\ \mathrm{j}k_z[N_{pi}(x, y) \end{bmatrix} \mathrm{e}^{\mathrm{j}k_z z}. \tag{8}$$

The $[B_p]$ matrix appears in the expression for the compressibility matrix $[\mathbf{H}]$,

$$[\mathbf{H}] = \iiint_{\Omega_f} K[B_p]^{*\mathrm{T}}[B_p]\, \mathrm{d}\Omega_f, \tag{9}$$

where K is the compressibility module. Changing the expression for $[B_{pi}]$ of equation (8) in the equation (9) allows one to write the $[H]$ compressibility matrix as

$$[H] = [H_0] + k_z^2[H_2], \tag{10}$$

where $[H_0]$ and $[H_2]$ are real symmetric matrices. The integration relative to the z variable introduces only the unit length. The compressibility matrix is calculated by integrating over the x and y variables on the cross-section S_f. Thus, the pressure field is z dependent but a bidimensional mesh, depending on x and y, is enough to calculate the compressibility matrix.

The mass matrix for the fluid domain is classically written as

$$[M_1] = \iiint_{\Omega_f} \rho_f[N_p]^{*T}[N_p]\, \mathrm{d}\Omega_f. \tag{11}$$

Because $[N_p]$ is of the form of equation (6), the mass matrix for the fluid domain is modified but is k_z independent. The $[M_1]$ matrix is calculated by integrating the x and y variables only on the S_f surface.

2.3.3. *Fluid–solid interface*

Because the whole domain contains a solid part and a fluid part, the $[L]$ matrix of the finite element formalism, which corresponds to the coupling between the solid and the fluid

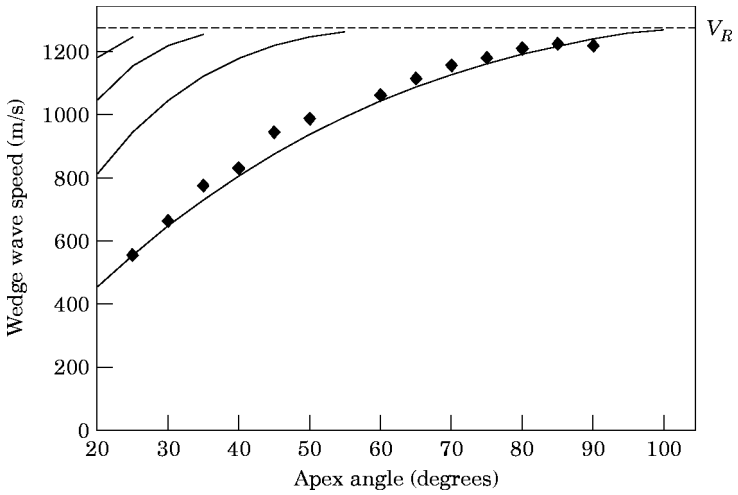

Figure 2. Variations of the wedge wave speeds, as a function of the apex angle of the Plexiglas wedge. ——, Finite element results; ◆, experimental results.

domains, has to be modified. Classically, this matrix is written as

$$[L] = \iint_{S_i} [N]^{*\mathrm{T}} \mathbf{n} [N_p] \, \mathrm{d}S_i, \tag{12}$$

where $\mathbf{n}$ is the normal vector to the S_i surface. The $[N]$ and $[N_p]$ matrices are the interpolation functions for the solid domain and for the fluid domain. Because the waveguide is uniform in the z direction, the normal vector to the interface element is in the x–y plane and has no component in the z direction. Thus, the coupling matrix is reduced to a curvilinear integral on the l_i line, which is the trace of the interface element in the x–y plane. This matrix is k_z independent.

2.3.4. *External fluid boundary*

Finally, because of the non-reflecting condition on the external fluid surface S_r, the trace of which in the x–y plane is the l_r line, the $[D]$ matrix relating the pressure normal derivative and the pressure on the surface has to be modified (see equation (4)). Classically, the $[D]$ matrix, for a monopolar pressure, is [10, 11]

$$[D] = \iint_{S_r} [N_p]^{*T} [N_p] \, \mathrm{d}S_r. \tag{13}$$

Using equation (6) for the expression of the interpolation functions in the fluid domain $[N_p]$ leads to a curvilinear integral on the l_r line. This matrix is k_z independent.

2.4. SOLUTION OF THE SYSTEM

From now on, all of the matrices appearing in the finite element system of equation (3) are written as a function of k_z. The whole system becomes

$$\begin{bmatrix} [K] - \omega^2[M] & -[L] \\ -\rho_f^2 c_f^2 \omega^2 [L]^{\mathrm{T}} & [H] - \omega^2[M_1] + \dfrac{\rho_f c_f^2}{R} [\tfrac{1}{2} - \mathrm{j}k_r R][D] \end{bmatrix} \begin{Bmatrix} \mathbf{U} \\ \mathbf{P} \end{Bmatrix} = \begin{Bmatrix} \mathbf{0} \\ \mathbf{0} \end{Bmatrix}. \tag{14}$$

With a view to calculating the angular eigenfrequencies of the system, the wavenumber k_z is given. By using a relation between the longitudinal wavenumber k_z and the radial wavenumber k_r on the external fluid boundary,

$$k^2 = k_r^2 + k_z^2 = \omega^2/c_f^2, \tag{15}$$

the terms depending on k_r are replaced in system (14). Upon using equations (5) and (10) and a variable change

$$\omega'^2 = \omega^2 - c_f^2 k_z^2, \tag{16}$$

equation (14) becomes

$$([A] + \omega'[B] + \omega'^2[C])\mathbf{X} = \mathbf{0}, \tag{17}$$

where

$$[A] = \begin{bmatrix} [K_0] + k_z[K_1] + k_z^2[K_2] - c_f^2 k_z^2[M] & -[L] \\ -\rho_f^2 c_f^4 k_z^2 [L]^{\mathrm{T}} & [H_0] + k_z^2[H_2] - c_f^2 k_z^2[M_1] + \dfrac{\rho_f c_f^2}{2R}[D] \end{bmatrix},$$

$$[B] = \begin{bmatrix} [0] & [0] \\ [0] & -\mathrm{j}\rho_f c_f [D] \end{bmatrix},$$

$$[C] = \begin{bmatrix} -[M] & [M_1] - [0] \\ -\rho_f^2 c_f^2 [L]^{\mathrm{T}} & \end{bmatrix} \quad \text{and} \quad \mathbf{X} = \begin{pmatrix} \mathbf{U} \\ \mathbf{P} \end{pmatrix}.$$

With a view to solving equation (17), the system is once again modified and is written as

$$\left(\begin{pmatrix} [0] & [A] \\ [A] & [B] \end{pmatrix} + \omega' \begin{pmatrix} -[A] & [0] \\ [0] & [C] \end{pmatrix} \right) \begin{pmatrix} \mathbf{X} \\ \omega' \mathbf{X} \end{pmatrix} = \begin{pmatrix} \mathbf{0} \\ \mathbf{0} \end{pmatrix}. \tag{18}$$

Finally, the system size is $2N \times 2N$, where N is the initial number of equations. For a given wavenumber k_z, the $[A]$, $[B]$ and $[C]$ matrices are built and the system is solved. The eigenvalues calculation gives the ω' values. Then, the angular eigenfrequencies ω and the radial wavenumber k_r are deduced, by using equations (16) and (15). The corresponding eigenvectors give the displacement field and the pressure field in the $z = 0$ plane. It is easy to reconstitute the displacement field and the pressure field in the $z = z_0$ plane by multiplying the eigenvectors by $\mathrm{e}^{\mathrm{j}k_z z_0}$. Finally, the propagation modes are characterized by their wave speed, which is the ratio between the angular eigenfrequencies and the k_z wavenumber.

3. IMMERSED PLEXIGLAS WEDGE

In this section, the variations of the wedge wave speed of Plexiglas linear wedges are studied, as a function of the apex angle. The physical constants of this material used for the calculation are a Young's modulus equal to $5{\cdot}85 \times 10^9$ Pa, a density equal to 1180 kg/m^3 and a Poisson ratio equal to 0·3343. The Rayleigh wave speed (V_R) is equal to 1271 m/s. The height of the wedges is large enough to be considered as infinite in the wavenumber band of interest. With a view to studying the antisymmetrical flexural modes, only half of the cross-section is meshed, by applying a specific boundary condition on the median plane. First, the wedge is in air and in Figure 2 are presented the variations of the wedge wave speed as a function of the apex angle. In all of the cases, the wedge wave

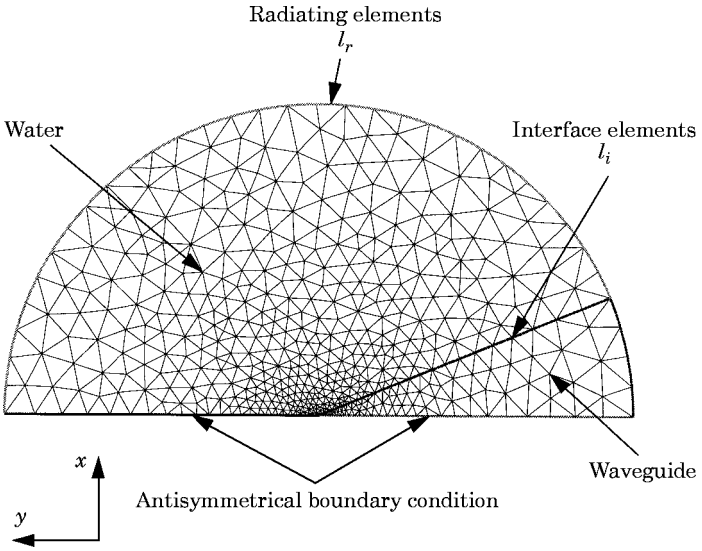

Figure 3. The finite element mesh of the immersed wedge.

speed is dispersionless and does not depend on the k_z wavenumber given for the calculation. In Figure 2, the experimental results [12] are indicated by a black square and concern only the fundamental mode. The continuous lines correspond to the variations of the wedge wave speed with respect to the wedge angle for the fundamental mode and for higher order modes. The agreement between the results is good. In the case of narrow apex angles, several antisymmetrical flexural modes exist [13]. As previously [4], the theoretical results show that antisymmetrical flexural modes exist only if the apex angle is smaller than 105°, which corresponds to a wedge wave speed smaller than the Rayleigh wave speed.

Then, the Plexiglas sample is immersed in water. In Figure 3 is presented the finite element mesh of the immersed wedge, containing a solid part, a fluid part, the interface

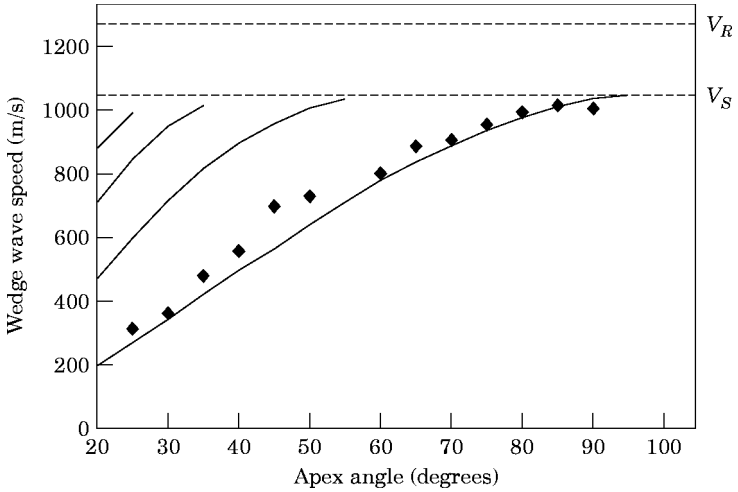

Figure 4. Variations of the wedge wave speeds, as a function of the apex angle of the immersed Plexiglas wedge. ——, Finite element results; ◆, experimental results.

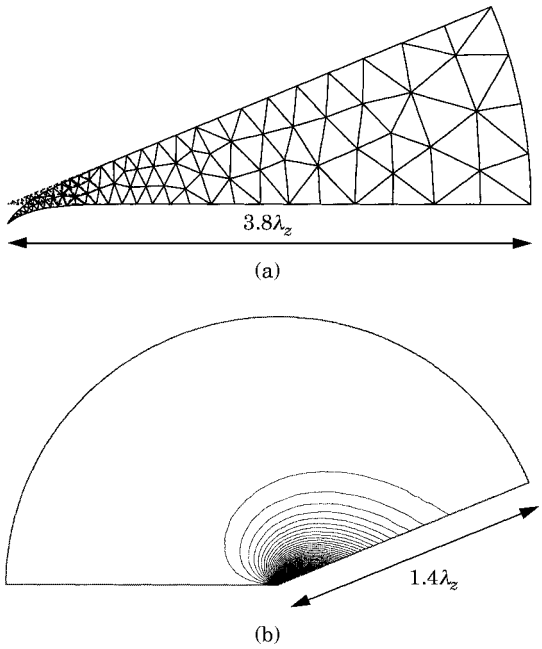

Figure 5. The first antisymmetrical wedge mode of a Plexiglas sample immersed in water. Half apex angle = 22·5°; $|k_rR| = 22{\cdot}2$. (a) The displacement field; dashed lines correspond to the rest position. (b) The pressure field in the x–y plane; the radius of the displayed fluid domain = $1{\cdot}4\lambda_z$.

line (l_i) between the fluid and the solid, and the radiating elements on the external line (l_r). Applying a monopolar condition on the external boundary of the finite element mesh, and for a given real k_z wavenumber, the angular eigenfrequencies are calculated. Then, the wedge wave speeds and the radial wavenumber k_r are deduced, from real angular eigenfrequencies. Therefore, the problem is limited to the propagating waves along the wedge, without re-emission in the fluid. Otherwise k_z should be taken to be complex, which has not been done in this study. A monopolar condition on the external fluid boundary is valid for the study of antisymmetrical wedge modes if $|k_rR|$ is large ($|k_rR| \gg 1$), which is experimentally verified. In Figure 4 are presented the variations of the wedge wave speeds of the immersed Plexiglas sample, as a function of the apex angle. In all of the cases, for the modes which are found by the finite element method, k_r is imaginary. Thus, the pressure field is exponentially decaying as a function of the distance to the tip. It corresponds to a located mode near the tip which is evanescent in the radial direction. Because k_r is imaginary and $|k_rR|$ is always greater than 1, the non-reflecting condition on the boundary is valid. The k_z wavenumber is real, which corresponds to a propagating mode in the z direction. Good agreement in Figure 4 is shown between the finite element results and the experimental data obtained for the first mode [12]. Comparing Figure 2 to Figure 4 shows that the water loading induces a decrease in the wedge wave speeds, which is greater for small apex angles. Because the Rayleigh wave speed is below the sound speed in water, all modes remain subsonic and there is no re-emission in the fluid. For 90° apex angle, the wedge wave speed is equal to 1034m/s. This value is close to the Stoneley–Scholte wave speed (V_S) [14] which is equal to 1044 m/s in Plexiglas. This latter wave propagates at the interface between the fluid and the solid and its speed V_S is analytically calculated [15]. Thus, the limit of the wedge wave speed in water for large apex angles is probably the Stoneley–Scholte wave speed.

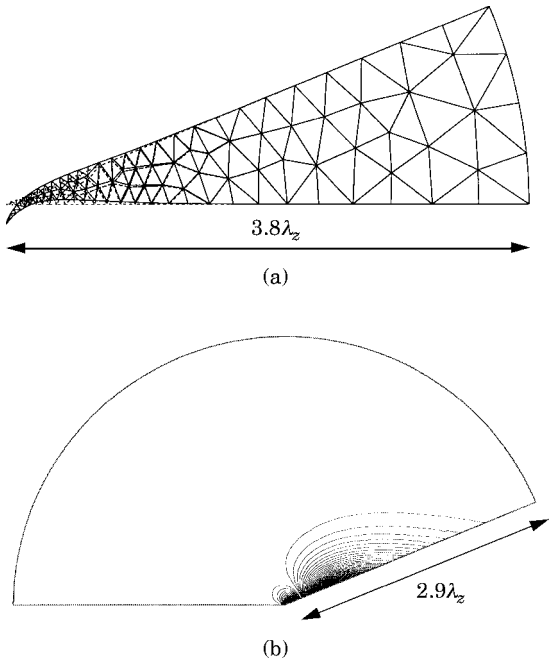

Figure 6. The second antisymmetrical wedge mode of a Plexiglas sample immersed in water. Half apex angle = 22·5°; $|k_r R| = 18{\cdot}3$. (a) The displacement field; dashed lines correspond to the rest position. (b) The pressure field in the x–y plane; the radius of the displayed fluid domain = $2{\cdot}9\lambda_z$.

In Figure 5(a) is presented the displacement field of the first antisymmetrical wedge mode in the x–y plane, for an apex angle of a Plexiglas wedge equal to 45°. It shows that the wave is located at the tip. In Figure 5(b) is presented the corresponding pressure field in the x–y plane in water, near the tip, at a distance smaller than $1{\cdot}4\,\lambda_z$, where λ_z is the wavelength in the wedge: the isovalues of the pressure are concentrated near the tip. In Figure 6(a) is presented the displacement field of the second antisymmetrical wedge mode

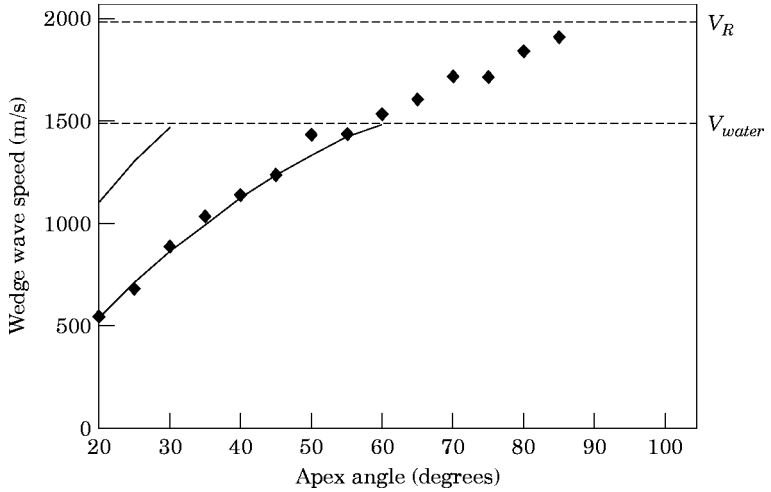

Figure 7. Variations of the wedge wave speeds, as functions of the apex angle of the immersed brass wedge. ——, Finite element results; ◆, experimental results.

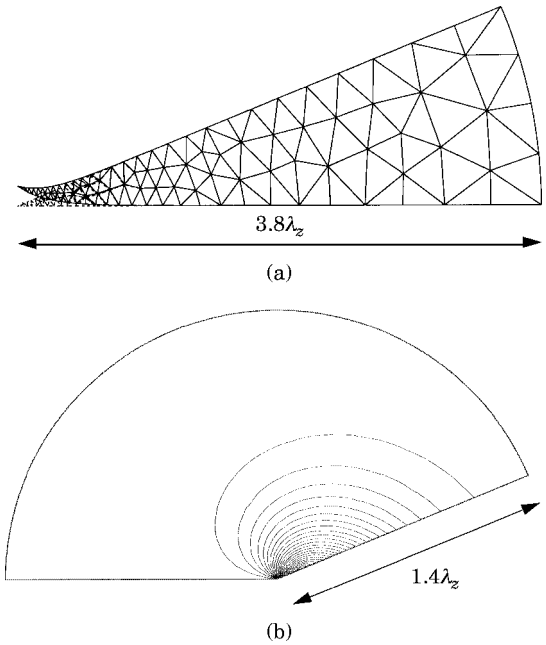

Figure 8. The first antisymmetrical wedge mode of a brass sample immersed in water. Half apex angle = 22·5°; $|k_r R| = 13{\cdot}5$. (a) The displacement field; dashed lines correspond to the rest position. (b) The pressure field in the x–y plane; the radius of the displayed fluid domain = $1{\cdot}4\lambda_z$.

in the x–y plane, for an apex angle equal to 45°. It shows that the wave is located at the tip. In Figure 6(b) is presented the corresponding pressure field in the x–y plane in water, near the tip, at a distance smaller than $2{\cdot}9\lambda_z$, where λ_z is the wavelength in the wedge: the isovalues of the pressure are concentrated near the tip. Because the mode is of a higher order, the pressure field presents two lobes, which correspond to two different phases of the pressure.

4. IMMERSED BRASS WEDGE

A brass linear wedge is now studied, as a function of the apex angle. The physical constants of this material used for the calculation are a Young's modulus equal to $1{\cdot}04 \times 10^{11}$ Pa, a density equal to 8600 kg/m^3 and a Poisson ratio equal to 0·3429. The Rayleigh wave speed (V_R) is equal to 1985 m/s. First, the wedge is in air and the variations of the wedge wave speed as a function of the apex angle are similar to those obtained on Figure 2.

The brass sample is then immersed in water. By using the finite element mesh of Figure 3, with a monopolar condition on the external fluid boundary and for a given real k_z wavenumber, the eigenfrequencies are calculated. Then, the wedge wave speeds and the radial wavenumber k_r are deduced. In Figure 7 are presented the variations of the wedge wave speeds of the immersed brass sample, as a function of the apex angle. In all of the cases, for the modes which are found by the finite element method, k_r is imaginary. Thus, the pressure field is exponentially decaying as a function of the distance to the tip. It corresponds to a mode located near the tip which is evanescent in the radial direction. The k_z wavenumber is real. Therefore, the problem is limited to the propagating waves, without re-emission in the fluid. Good agreement is shown in Figure 7 between the finite element

results and the experimental results [12]. Once again, the water loading induces a decrease in the wedge wave speeds, which is greater for small apex angles. In Figure 7 it is shown that the propagating modes in the z direction exist only if the wedge wave speed is below the sound speed in water. Therefore, for apex angles greater than 60°, wedge modes are not found with the finite element method. In fact, these modes are supersonic: they are attenuated in the wedge direction and radiating in the radial direction. Thus, with a given real k_z wavenumber, they are not found. The displacement field of the first antisymmetrical wedge mode in the x–y plane, for an apex angle equal to 45°, is presented in Figure 8(a). It shows that the wave is located at the tip. In Figure 8(b) is presented the corresponding pressure field in the x–y plane in water, near the tip, at a distance smaller than 1.4 λ_z, where λ_z is the wavelength in the wedge: the isovalues of the pressure are concentrated near the tip. If the apex angle is equal to 45°, only one wedge mode is found, because the second corresponds to a wedge wave speed greater than the speed of sound in water.

5. CONCLUSIONS

In this paper a detailed analysis has been presented of the propagation of acoustic waves in immersed linear waveguides. Results computed with the ATILA code have demonstated the ability of the finite element method to predict the propagation of acoustic waves in immersed guides, and good agreement has been found between results obtained by the finite element models and by measurements. Moreover, the efficiency and versatility of this finite element approach have been demonstrated. Indeed, modifying the waveguide requires only the modification of the mesh of the cross-section, without any development related to the method. Moreover, any isotropic or anisotropic material, if the anisotropy respects the symmetry condition in the waveguide direction, can be considered.

When the samples are immersed, the effect of the water loading induces a decrease in the wedge wave speed. If the resulting speed is subsonic, it corresponds to a mode which is propagative in the wedge direction and evanescent in the radial direction. For 90° apex angle, the wedge wave speed limit is the Stoneley–Scholte wave speed. These modes are found with the finite element method, because they correspond to a given real wavenumber in the wedge direction. If the resulting mode is supersonic, it is attenuated in the wedge direction but is radiating in the radial direction. This latter mode has not yet been found with the finite element method, because the given wavenumber in the wedge direction is complex. One of our aims is now to extend this technique to any wavenumber, with a view to finding either propagating wedge modes or attenuating wedge modes with the finite element method. In that case, the way to find all modes is to calculate the wavenumbers k_z and k_r for a given angular frequency ω. This work is now in progress.

ACKNOWLEDGMENT

The authors wish to thank Dr Bossut, from the IEMN, Département ISEN, for his help with the algorithm and program developments.

REFERENCES

1. E. A. Ash, R. M. de la Rue and R. F. Humphryes 1969 *IEEE Transactions on Microwave Theory and Techniques* **MTT-17**, 882–892. Microsound surface waveguides.
2. S. L. Moss, A. A. Maradudin and S. L. Cunningham 1973 *Physical Review B* **8**, 2999–3008. Vibrational edge modes for wedges with arbitrary interior angles.

3. P. E. Lagasse 1973 *Journal of the Acoustical Society of America* **53**, 1116–1122. Higher-order finite element analysis of topographic guides supporting elastic surface waves.
4. A.-C. Hladky-Hennion 1996 *Journal of Sound and Vibration* **194**, 119–136. Finite element analysis of the propagation of acoustic waves in waveguides.
5. V. V. Krylov 1994 *IEEE Ultrasonics Symposium*, 793–796. Propagation of wedge acoustic waves along wedges imbedded in water.
6. J. R. Chamuel 1991 *Sonoquest Advanced Ultrasonic Research*, *Report JRC*-34-91. Ultrasonic studies of transient seismo-acoustic waves in bounded solids and liquid/solid interfaces.
7. J. R. Chamuel 1993 *IEEE Ultrasonics Symposium*, 313–318. Edge waves along immersed elastic elliptical wedge with range dependent apex angle.
8. J. N. Decarpigny 1984 *Thesis*, *Université des Sciences et Techniques de Lille*. Application de la méthode des éléments finis à l'étude de transducteurs piézoélectriques.
9. O. C. Zienkiewicz 1977 *The Finite Element Method*. New York: McGraw-Hill.
10. J. Assaad 1992 *Thesis*, *Université de Valenciennes et du Hainaut-Cambrésis*. Modélisation des transducteurs piézoélectriques haute fréquence à l'aide de la méthode des éléments finis.
11. P. M. Morse and H. Feshback 1953 *Methods of Theoretical Physics*. New York: McGraw-Hill.
12. M. de Billy 1996 *Journal of the Acoustical Society of America* **100**, 659–662, On the influence of loading on the velocity of guided acoustic waves propagating in linear acoustic wedges.
13. P. E. Lagasse, I. M. Mason and E. A. Ash 1973 *IEEE Transactions on Microwave Theory and Techniques* **MTT-21**, 225–236. Acoustic surface waveguides—analysis and assessment.
14. J. G. Scholte 1949 *Proc. Kon. Ned. Akad. Van Wetensch.*, *Amsterdam* **52**, 652–653. On true and pseudo-Rayleigh waves.
15. J. Guilbot 1994 *Thesis*, *Institut National des Sciences Appliquées de Lyon*. Caractérisation acoustique de fonds sédimentaires marins par étude de la dispersion de célérité des ondes d'interface de type Stoneley–Scholte.